Research on Engineering Structures & Materials
www.jresm.org
Research Group

Research Article

Axial performance, stiffness, and failure modes of circularly tapered non-prismatic reinforced concrete columns

Romaih O. Mostafa [*,a], Sofyan Y. Ahmed [b], Jasim A. Abdullah [c]

Department of Civil Engineering, College of Engineering, University of Mosul, Mosul, Iraq

Article Info

Article History:

Received 03 Sep 2026

Accepted 30 Oct 2026

Keywords:

Non-prismatic RC columns;
Circular taper;
Axial compression;
Bi-axial compression;
Confinement effect;
Failure modes;
Energy dissipation

Abstract

Most structural codes focus on prismatic columns, often overlooking the benefits of non-prismatic shapes. This study investigates how reinforced concrete columns tapered along a circular arc behave compared to standard prismatic ones under axial loads. Four specimens were tested (2 prismatic and 2 non-prismatic). Using 1.5m height specimens with equal reinforcement (6φ10) and a constant depth of 150mm, the experimental program tested columns that varied their width from 300mm at the ends to 150mm at mid-height as non-prismatic columns, whereas the prismatic columns had a section of 150mm x 150mm. Results revealed that non-prismatic columns have a higher load carrying capacity than prismatic columns by 17.90% and improved axial stiffness by at least 74.03%. Notably, while prismatic columns failed in the upper half, tapered specimens failed at the necking region, demonstrating a more efficient use of the entire member. Additionally, the strain in the curved rebars was 66% of that recorded in prismatic members at equivalent load level. Although non-prismatic columns dissipate less energy than prismatic specimens (1306.71J compared to 2137.33J) and exhibited a more brittle response, they maintained superior lateral stability. Within the limits of the tested specimens, this study supports that the circularly tapered shape increases strength due to improved confinement provided by bi-axial compressive stress within the column, thereby offering a more efficient method for structural design.

© 2026 MIM Research Group. All rights reserved.

1. Introduction and Research Significance

Non-prismatic reinforced concrete columns have cross-sections that vary continuously or in steps along their height. Continuous variations in cross-sectional area and moment of inertia impede straightforward analytical derivations, compelling analysts to resort to complex numerical approximations [1,2]. While the number of studies on tapered columns is limited and their findings may not be generalized, several published research efforts have explored this topic. Most of these studies have concentrated on the linearly tapered columns [3-5]. Pedreschi [6] investigated the axial behavior of concave and convex tapered columns compared them to the conventional columns, concluding that concave profiles sustained up to 90–100% greater axial load than prismatic controls of equal concrete volume. Convex columns with increased mid-point diameters carried the least load, attributed to shape influence on lateral tensile strain development. The parabolic geometry (concave) of the column has particular advantages in that it creates a state of biaxial compression at the mid height of the column, preventing cover spalling, premature cracking, and enhancing the confinement in concrete. This fact is confirmed by the strut and tie model described by He Z. Q. et al. [7].

Al-Maliki & Mahmood [4] investigated the behavior of RC linearly tapered columns under axial loading. The study concluded that the solid section has a higher strength capacity as the main reinforcement increases. Some studies have focused on the numerical analysis and validation of

*Corresponding author: romaih.23enp54@student.uomosul.edu.iq
[a]orcid.org/0009-0001-4100-0889; [b]orcid.org/0000-0001-8394-6157; [c]orcid.org/0000-0002-2245-560X
DOI: http://dx.doi.org/10.17515/resm2026-2286st0903rs

linearly tapered columns [5,8,9]. Kadhim & Al Zaidee [9] concluded that the slenderness ratio of RC linearly tapered columns can be reliably evaluated using ACI Code formulae with the average cross-section of the tapered member. Some published studies have proposed methods for analyzing and designing non-prismatic reinforced concrete columns [10-12]; however, these methods have not been validated in international codes. To report further information, it is necessary to perform more studies on the structural behavior of such types of columns.

Current international structural design codes (e.g., ACI 318-19, Eurocode 2) primarily focus on conventional columns with uniform cross-sections, lacking explicit provisions for non-prismatic members. Pedreschi attributed the reasons for high load carrying capacity in concaved columns to the influence that shape has on the development of lateral tensile strains in the columns. The current study intends to verify Pedreschi's findings and identify the mechanical reasons for this enhancement. The objective of the current study is to investigate the behavior of columns of variable cross-section (tapered along a circular arc) and comparing them to the constant cross-section columns under concentric axial load, and systematically evaluate both the structural advantages and mechanical trade-offs (such as load-carrying capacity, stiffness, stress distribution, and the expected failure location.

2. Experimental Program

The experimental program includes selecting and testing materials necessary to construct the reinforced concrete columns, curing of concrete, and testing the specimens.

2.1 Materials

2.1.1 Concrete Ingredients

Ordinary Portland Cement (OPC) of 32.5 grade, complying with Iraqi Standards IQS: NO.5/2019 [13], was used for making concrete. The maximum size of the coarse aggregate is (12.5mm). River sand and gravel were graded, complying with Iraqi Standards IQS: NO.45/2016 [14]. Table 1 shows the concrete mix proportions used throughout the study and the average of three standard cylinders (6 by -12 in.) compressive strength of concrete at 28 days according to ASTM C39/C39M-24. The measured slump of the mix was 140mm

Table 1. Concrete mix proportions per 1m3 and the compressive strength of concrete

Cement (kg)	Fine Aggregate (kg)	Coarse Aggregate (kg)	Water (kg)	w/c ratio	28 days f'c (MPa)
360	870	970	153	0.425	28.5

2.1.2 Reinforcing Steel

Deformed steel bars (φ10 mm main reinforcement, φ8 mm stirrups) conforming to ISO 6935-2-2019 [15] for grade B500B-R and B300D-R respectively were used. Tensile testing showed an average yield strength of 627 MPa and 307 MPa for two respective diameters. The significant difference in yielding strength came from the types available in the local markets. The arrangement of transverse reinforcement was in accordance with ACI318-19 (18.4.3.3) [16], where the reinforcement was φ8@75mm over a length of 250mm at the column ends, while the distribution was φ8@140mm over the middle length of the column. The tensile test was performed in the laboratory of materials testing/ Civil Eng. Dept./University of Mosul. The mechanical properties of the reinforcing rebars are listed in Table 2.

Table 2. Mechanical properties of reinforcing rebars

Bar diameter	10 mm	8mm
Yield Tensile Strength (N/mm2)	627	307
Ultimate Tensile Strength (N/mm2)	696	447
Strain at Yield (E=200000MPa)	0.003135	0.001535

2.1.3 Carbon Fiber Reinforced Polymer (CFRP)

According to many publications [17] [18] [19], the use of CFRP in the rehabilitation and strengthening of concrete members offers a number of clear advantages over conventional techniques like steel or concrete jacketing. To overcome the local failure due to bearing stresses, the column ends were wrapped with one single layer of unidirectional CFRP fabric along the circumferential direction over a height of 150 mm in accordance with ISO 10618, produced by Don Construction Products (DCP- Profiber CW 300 system). The surface of the column was primed by Quickmast Primer CW which has an adhesive strength > 1.5 MPa according to the products' data sheet. 24 hours curing time later, the mixed Quickmast ER350 (tensile strength >25 MPa, adhesive strength >3.5 MPa, the compressive strength >60 MPa, and the tensile elongation at break >3%) was applied to the prepared substrate. Within the open time of the adhesive resin (15-30 min), the Profiber CW System fabric was placed onto the resin in the required direction. The depth of wrapping was 150mm, and the lap splice was 100mm. Table 3 shows the mechanical properties of Profiber CW300

Table 3. The mechanical properties of the Profiber CW300

weight (g/m2)	Design thickness (mm)	Tensile strength (MPa)	Tensile E-Modulus (GPa)	Elongation at break (%)
300	0.166	4800	230	1.7

2.2 Description of Specimens

Two prismatic columns (PRIS-0, PRIS-1) were constructed. The cross-section is (150x150) mm, and the height is 1500 mm. Whereas, the non-prismatic specimens (NPRIS-0, NPRIS-1) were fabricated with a circular-arc profile (R = 2438 mm), the varied width is governed by $w(x)/2 = 75 + R - \sqrt{(R^2 - x^2)}$ (mm) for $|x| \leq 600$ mm. A constant depth of 150mm is considered, and the total height is 1500mm. The concrete cover is 25mm for all specimens on all sides. Fig. 2 shows the geometry of the non-prismatic and prismatic columns. The main bars were bent to conform to the outer curvature by skilled laborers using rebars bending machine and the residual stresses were not measured during the bending process. Table 4 shows the specimens' characteristics.

Table 4. Characteristics of specimens

Designation	Width/depth (mm)	Height (mm)	Clear concrete cover (mm)	Reinforcement ratio %
PRIS-0	150/150	1500	25	2.09
PRIS-1	150/150	1500	25	2.09
NPRIS-0	w1/150	1500	25	1-2.092
NPRIS-1	w1/150	1500	25	1-2.092

Note: The width of the specimens changes according to equation $w(x)/2 = 75 + R - \sqrt{(R^2 - x^2)}$, The reinforcement ratio changes from 1% at both ends to 2.09% at mid height.

2.3 Measuring Devices

The universal testing machine available in the materials testing laboratory/civil engineering department/ University of Mosul, shown in Fig. 3, was used to apply the axial compression load on the column specimens. The capacity of the testing machine is 1500 kN. A 1500kN load cell was attached to the hydraulic jack and connected to the 16-channel data logger. To measure the axial and lateral displacements, three transducers (LVDT) were installed as shown in Fig. 3 and connected to the same data logger. To monitor the strain in the reinforcing rebars during loading, two strain gauges were attached to each specimen. One on the main rebar (815mm and 750mm above the bottom face of prismatic specimens and the non-prismatic specimens, respectively) and the other on the stirrup (1185mm and 958mm above the bottom face of prismatic specimens and the non-prismatic specimens, respectively) as shown in Fig. 1. A limited number of strain gauges is

considered just to investigate strain where the failure is expected to occur. The specifications of the strain gauges are illustrated in Table 5.

Table 5. Strain gauges specifications

Type	Length (mm)	Lead wires (Ω/m)	Gauge factor	Gauge resistance (Ω)	Manufacturer
FLAB-6-11-3LJC-F	6	10/0.12 2w 3m r=0.32	2.12±1%	118.5±0.5	TML/ Japan

2.4 Effect of the Column Slenderness

The slenderness ratio (λ) of the prismatic column according to ACI 318-19 (Section 6.2.5.1a) [16], the slenderness ratio is calculated via Eq. (1):

$$\lambda = \frac{kL}{r} = \frac{1 \times 1500}{0.3 \times 150} = 33.33 \ > 22 \tag{1}$$

where k is the effective length factor, L is the unsupported height of the column, and r is the radius of gyration. The column is unbraced, and the slenderness ratio exceeds 22, so the prismatic column is classified as a slender column.

To simplify the integration and to obtain the equivalent moment of inertia in closed form for the non-prismatic specimens, the circular profile was idealized by the following parabola:

$$w(x)/2 \ = \ (0.20833)\, x^2 \ + \ 0.075 \tag{2}$$

where (x and w in meters, x measured from mid-height). This parabola deviates from the circular arc by less than 0.3 mm over the tapered length. Using the Rayleigh energy method with an assumed sinusoidal mode [20] for pin-ended conditions gives Ieq/Imin ≈ 1.2025 for flexure across the constant depth. The corresponding effective slenderness ratios are approximately 30.4, compared with 33.3 for the prismatic column. The non-prismatic columns therefore remain slender. Because these values are based on gross elastic properties and the longitudinal reinforcement is constant along the height, they should be regarded as upper bounds.

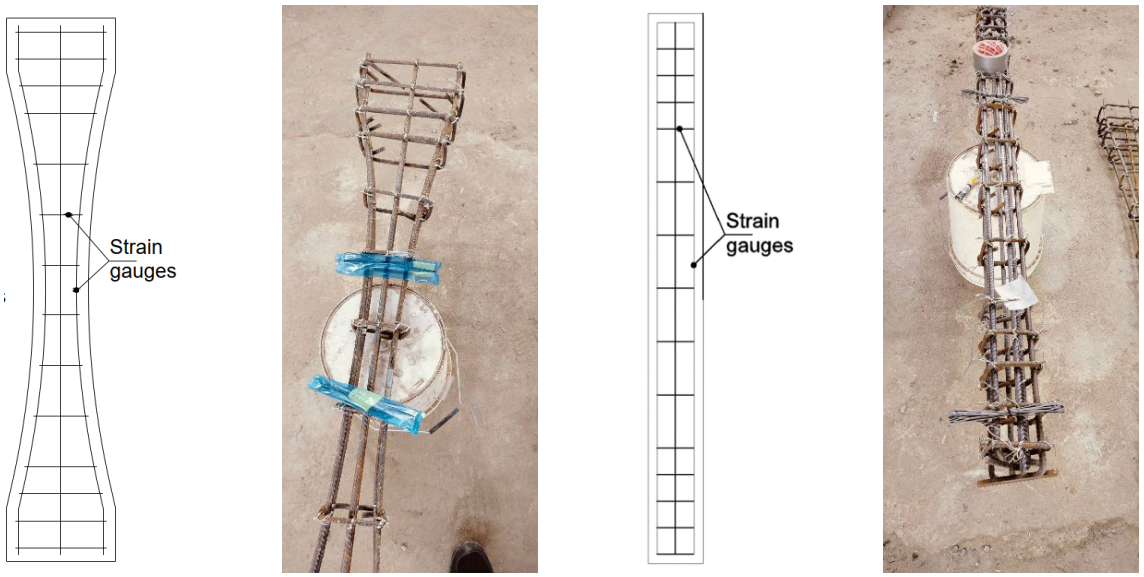
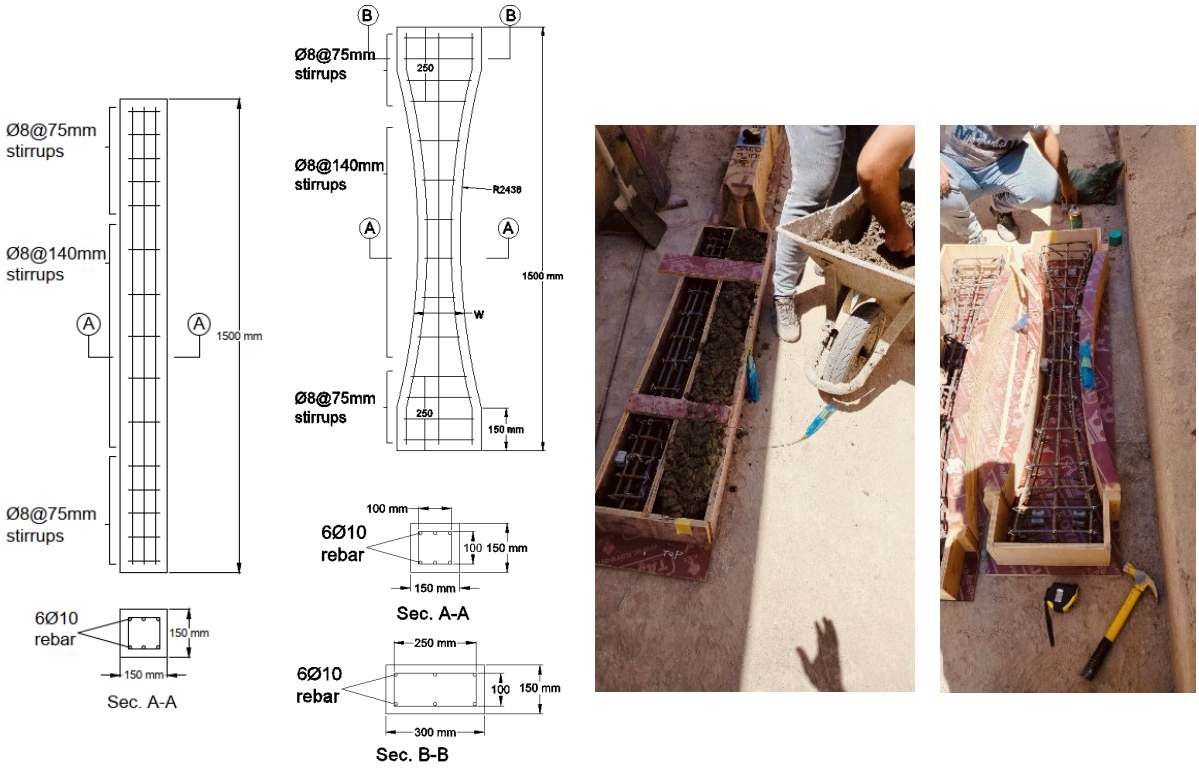


Fig. 1. Strain gauge locations and instrumented reinforcement cages



a) Specimens geometry b) Fabrication of the specimens

Fig. 2. The geometry and fabrication of specimens

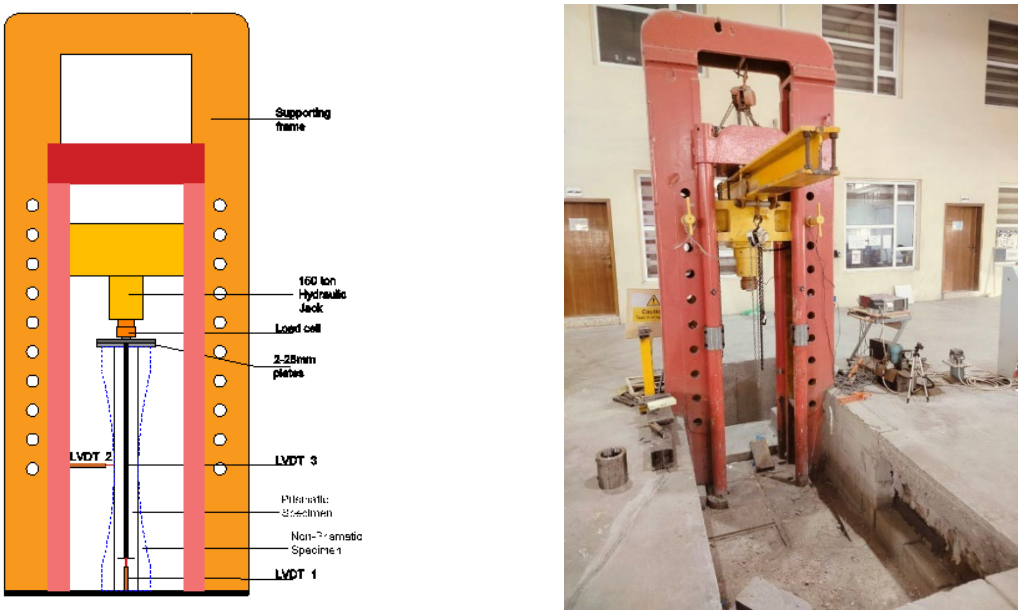


Fig. 3. Universal testing machine

2.5 Boundary Conditions at the Ends of the Specimens

The bottom end of the specimen was placed directly on the rigid base of the universal testing machine. 2-25mm steel plate were placed on the top end of the specimen as shown in Fig.3. The friction between specimen faces and the attached plates prevents the specimen from translating laterally. So, both ends are pinned.

3. Results and Discussion

Experimental outcomes obtained from the physical testing of four reinforced concrete (RC) columns, are presented and discussed below:

3.1 Axial Load Capacity

The two non-prismatic specimens (NPRIS-0, NPRIS-1) were tested under compression up to failure at a rate of loading of 1.75kN/sec. The average load-carrying capacity was 905.1 kN. In addition, the two prismatic specimens (PRIS-0 & PRIS-1) were loaded at a rate of loading of 1.75kN/sec. They showed an average load-carrying capacity of 767.65 kN. The results of testing specimens are listed in Table 6. Nonprismatic specimens show approximately 17.90% more axial load than the prismatic counterparts before failure. This is consistent with a geometric/ mechanical explanation rather than a material-based one, since the concrete batch and reinforcement ratio were nominally identical between the two groups. The interpretation of this increase is attributed to the geometry of non-prismatic specimens which confines the concrete at the middle half of the specimen and creates a state of biaxial stress which raises the compressive strength of concrete. This phenomenon is stated in the literature, especially the study performed by Kupfer H. et al. [21] and the strut and tie model created by He ZQ, et. al [7]. The wider ends provide a larger "bearing" zone, which helps distribute the high-intensity stresses from the testing machine more uniformly into the core.

Table 6. The outcomes of the axially loaded test

Specimen	NPRIS-0	NPRIS-1	Average	PRIS-0	PRIS-1	Average
Failure load (kN)	854.4	955.8	905.1	775.7	759.6	767.65
Load at yielding of the rebar (kN)	Not yield	Not yield		741	722	731.5
Axial displacement at max. load (mm)	3.04	3.86	3.45	6.53	4.16	5.35
Lateral displ. at max. load LVDT2 (mm)(width)	---	---	---	0.31	0.49	0.4
Lateral displ. at max. load LVDT3 (mm)(depth)	1.04	0.53	0.785	1.65	1.86	1.755
Strain in the rebar at max. load	0.0026	0.0028	0.0027	0.0036	0.0034	0.0035
Strain in the stirrup at max. load	0.0014	0.0015	0.00145	0.0014	0.0014	0.0014

Eccentricity in columns is unavoidable, Nevertheless, Section 22.4.2.2 of ACI 318-19 defines the nominal axial strength at zero eccentricity (Po), as expressed in Eq. (3), for the smallest section (150x150mm) is 829 kN which lower than that recorded by the non-prismatic columns by 9%. Once again, the reason for this increase is that the concrete compressive strength at the necking region has been increased as a result of the confinement caused by the geometry:

$$Po = 0.85fc'(Ag-Ast) + fy\,Ast = 829\ kN \quad (3)$$

A difference of approximately 11.9% was observed between the two non-prismatic specimens (854.4 kN for NPRIS-0 and 955.8 kN for NPRIS-1), compared with only 2.1% between the prismatic specimens. Several factors are considered responsible. First, the tapered geometry forces failure at the single minimum section at mid-height, so the capacity of a non-prismatic column depends on the concrete quality in a small critical volume. In a prismatic column, by contrast, the governing section is the weakest of many equally stressed sections along the height. Second, NPRIS-0 also showed lower axial stiffness [12%, Table 6], lower axial displacement at peak load (3.04 vs 3.86 mm) and lower toughness than NPRIS-1. This consistent reduction suggests locally lower concrete quality at the neck, which may result from more difficult compaction where the arched longitudinal bars and stirrups converge in the 150 mm section during horizontal casting. Third, at peak load NPRIS-0 exhibited approximately twice the mid-height lateral displacement of NPRIS-1 in the

depth direction measured by LVDT3 (1.04 vs 0.53 mm; Table 5). This is the direction of the minimum constant dimension and therefore the governing buckling direction, indicating a larger accidental eccentricity or initial imperfection in NPRIS-0. A simple elastic estimate indicates that an eccentricity of only about 2.5–3 mm at the 150 mm neck can reduce the capacity by about 10%, which is why design codes allow for accidental eccentricity (ACI, 2019). Despite this scatter, the weaker non-prismatic specimen (854.4 kN) still exceeded the stronger prismatic specimen (775.7 kN) by 10.2% and exceeded the nominal axial strength of the minimum section (P_0 = 829 kN). The strength advantage of the non-prismatic geometry is therefore not an artefact of specimen variability.

3.2 Failure Mode

The four specimens failed suddenly without any warning. No major macro-cracks were visually observed prior to peak load. The inclined failure plane shown in Fig.4 is an indication of shear/crushing failure (compression crushing along an inclined plane / diagonal tension). Failure began with shear in concrete, followed by crushing of concrete due to a reduction in the cross-sectional area, and finally spalling of concrete cover and buckling of main reinforcing bars. The failure of non-prismatic columns occurred at mid-height. While it was located in the upper half in the prismatic columns. This indicates that the geometry of the non-prismatic column successfully utilized the full capacity of the entire member, forcing the failure to the theoretical point of maximum demand (mid height) only after the column had reached a much higher total load. Unlike the prismatic columns the failure location of the non-prismatic columns is predictable and localized at the minimum (neck) section, where the axial stress is greatest.



a) Mid-height necking failure in non-prismatic columns

b) Upper-half failure in prismatic reference columns

Fig. 4. Failure modes of tested specimens

3.3 Axial Stiffness and Energy Dissipation

Fig. 5 shows the load-deflection curves of the tested specimens. The stiffness was calculated based on the slope of the secant line connecting the origin to the point where the load reaches 600 kN, since the behavior of the specimens was relatively linear within this range. The non-prismatic columns exhibit 74% stiffer behavior than prismatic columns on average. This is due to increasing width of the proposed geometry, which enhances the axial stiffness of the specimen as stated in Table 6. However, this increase in stiffness translates into a more brittle structural response, which is critical for buildings in seismic zones or areas exposed to severe impacts.

Also, Table 7 shows the energy dissipated (toughness) by the specimens. Non-prismatic columns, despite their stiffness, lose energy and fail earlier. The dissipated energy by non-prismatic specimens was 61.14% compared to the prismatic specimens. The greater axial shortening and subsequent ductility observed in the PRIS series can be attributed to the interaction between axial compression and lateral deflection.

Table 7. Axial stiffness and toughness indices of the tested specimens

Specimen	Axial stiffness (kN/m)	Average	Toughness (J)	Average
PRIS-0	157,986	190,116	2,746.35	2,137.33
PRIS-1	222,247		1,528.31	
NPRIS-0	312,100	330,874	1,156.14	1,306.71
NPRIS-1	349,649		1,457.28	

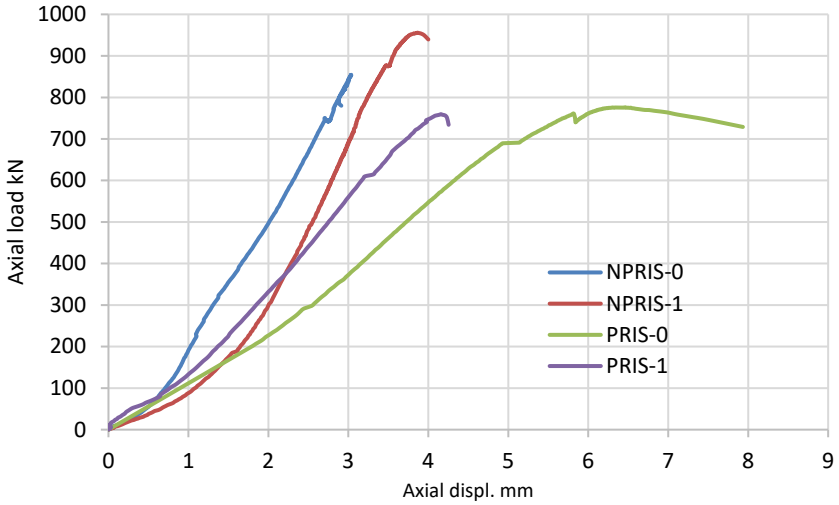


Fig. 5. Axial load-axial deflection behavior for the tested specimens

3.4 Lateral Deflection

Fig. 6 shows the axial load versus lateral deflection behavior at the mid-height of the column. The lateral deflection was recorded by LVDT3 along the weak axis of the non-prismatic specimens. The lateral deflection in non-prismatic columns does not increase with an increase in axial load. To a certain extent, it can be said that lateral deflection is relatively constant during an increase in axial load. The lateral deflection in a prismatic column is monotonic. In other words, the flexure behavior, which is clearly visible in prismatic columns as a result of the slenderness effect, is limited and has less impact on non-prismatic columns. The flexural stiffness of prismatic columns degraded early at 40%-60% of the maximum strength capacity. While in non-prismatic columns, the flexural stiffness remains constant up to 85% of the maximum strength capacity, as specimen (NPRIS-1) shows.

3.5 Axial Strain in the Main Reinforcement

Fig. 7 displays the axial strain in the reinforcing rebar at locations specified in Fig. 1. Obviously, the strain in non-prismatic columns is less than that in prismatic columns. At the failure load level in the prismatic columns (at about 758kN), the strain in the non-prismatic columns is about 66% of that in the prismatic columns. This can be attributed to the larger cross-section of concrete in non-prismatic specimens, which carry more load and consequently reduce the load transferred to the reinforcing rebar. Table 5 shows that the strain in reinforcing rebar in non-prismatic specimens did not yield before the ultimate load, while it yielded in prismatic specimens. This behavior led to the brittle failure mode because the majority of load was carried by the concrete. To change this mode into more ductile behavior the reinforcement ratio can be reduced or considered as a parameter in the upcoming studies.

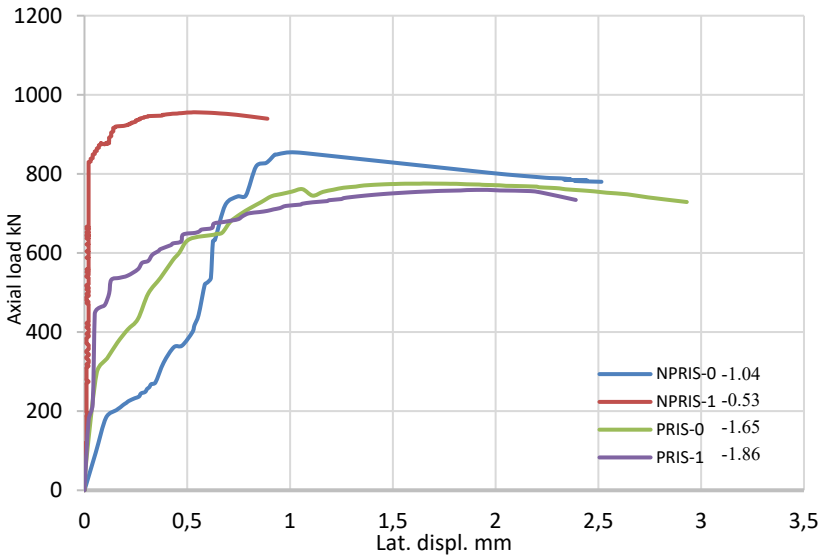


Fig. 6. Axial load- lateral displacement behavior for the tested specimens

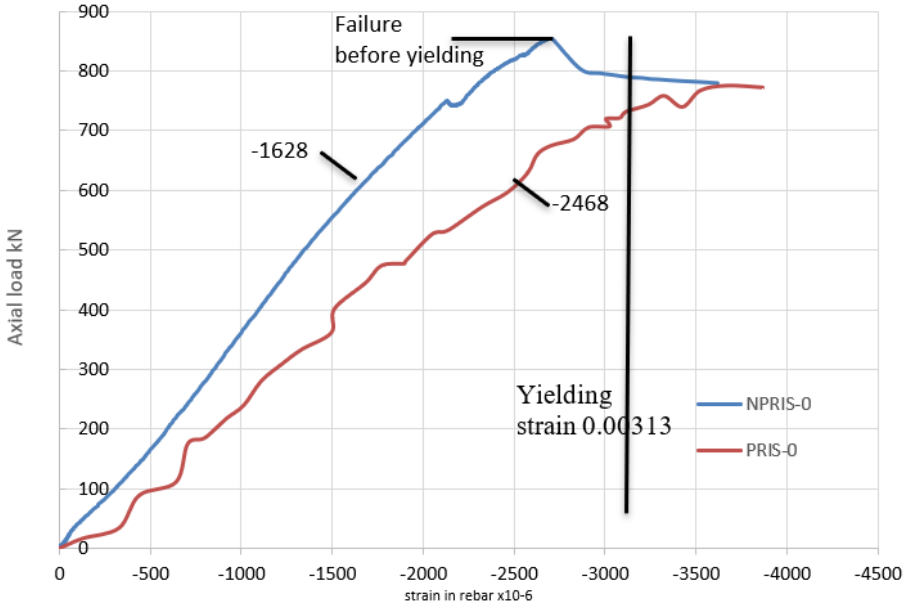


Fig. 7. Axial load vs recorded strain in the main rebar

4. Conclusions

The current study concluded that the reinforced concrete columns of circular tapered geometry showed a positive impact on the strength, load carrying capacity, stiffness, stability, and predicted location of failure compared to the conventional columns. while, it showed a brittle response as it fails with less dissipated energy. These conclusions come from the study findings illustrated below:

- Circular tapered geometry applies biaxial compression to the concrete: The load-carrying capacity under axial compression in the non-prismatic columns was 17.90% higher than that of prismatic ones. This behavior is due to the circular geometry of non-prismatic specimens, which subjects the concrete to a biaxial compression condition which raises the effective compressive strength of the concrete and reduces the effect of the lateral expansion at mid height of the specimens. As a result, the onset of microcracks and internal collapse is delayed.
- Circular tapered geometry increases the axial and flexural stiffness: Experimentally, the tapered geometry raised axial stiffness by about 74% higher than that of prismatic ones. This is due to the effect of increasing width of the proposed geometry. Varying the width makes the critical section larger than the smallest one. According to Rayleigh energy method, the calculated equivalent moment of inertia of considered specimens increased by 20.25%

comparing to the smallest section causing a reduction in the slenderness ratio from 33.333 to 30.4.

- Necking region localizes the critical section: The location of failure in the non-prismatic columns was at the middle height (necking region), while prismatic columns failed within the upper half of their height. This means that the failure location of the non-prismatic columns is predictable and localized at the minimum (neck) section, and adds a positive feature to the non-prismatic columns, where the strengthening and repair activities can be applied only at this location.
- Circular tapered column shows better stability: Prismatic columns showed early reduction in flexural stiffness (at 40%–60% of their maximum capacity). While the non-prismatic columns maintained their initial flexural stiffness up to 85% of their maximum load.
- The wider ends relieve the bearing stress: The axial strain in the longitudinal rebars in the non-prismatic columns was 66% of that recorded in the prismatic columns at the load of 758 kN. This comes from the larger section of the column at the upper face, where the concrete bears the majority of the applied load.
- Greater stiffness causes the material's behavior to tend toward a brittle response: The energy dissipated by the non-prismatic specimens formed 61.14% of the energy dissipated by the prismatic specimens. This brittle behavior is attributed to the increase in stiffness mentioned above.
- While parabolically tapered RC columns offer significant advantages in axial load capacity and stiffness, their reduced energy dissipation capacity and brittle failure behavior necessitate caution in seismic design. They are primarily recommended for gravity-load-dominated structures or bridge bents where high axial rigidity is prioritized over energy dissipation.

4.1 Limitations and Recommendations for Future Work

Because only four specimens were tested, the following research needs are identified:

- More specimens and effect. Larger test series with more replicates per configuration, to establish statistical reliability and to address the scatter observed between the two non-prismatic specimens (≈11.9%).
- Eccentric loading. Tests under uniaxial and biaxial eccentricity, to build axial load–moment interaction diagrams for non-prismatic columns and to check whether the confinement benefit persists under combined axial load and bending.
- Parametric finite element analysis. Numerical models validated against these tests (e.g. concrete damaged plasticity), used to study taper ratio, arc radius, longitudinal and transverse reinforcement ratios, concrete strength, slenderness, and equal-concrete-volume comparisons.

Acknowledgement

The authors acknowledge that this study is supported by University of Mosul/College of Engineering/Civil Engineering Department.

References

[1] Mercuri V, Balduzzi G, Asprone D, Auricchio F. Structural analysis of non-prismatic beams: critical issues, accurate stress recovery, and analytical definition of the Finite Element (FE) stiffness matrix. Engineering Structures. 2020;216:110252. https://doi.org/10.1016/j.engstruct.2020.110252

[2] Gesteira ASA, Martha LF, Burgos RB. Finite elements formulation for non-prismatic frames. In: Proceedings of the XLV Ibero-Latin-American Congress on Computational Methods in Engineering (CILAMCE 2024); 2024 Nov 11-14; Maceió, Brazil. ABMEC; 2024.

[3] Brant NFA. Reinforced concrete columns of variable cross section [doctoral dissertation]. London: The City University; 1984.

[4] Al-Maliki HNG, Mahmood MS. Structural Behavior Investigation of Reinforced Concrete Tapered Solid and Hollow Section Columns under Axial Load. Association of Arab Universities Journal of Engineering Sciences. 2018;25(2):1-18.

[5] Kadhim JA, Al Zaidee SR. Validated three-dimensional finite element modeling for static behavior of RC tapered columns. Journal of the Mechanical Behavior of Materials. 2023;32(1):20220226. https://doi.org/10.1515/jmbm-2022-0226
[6] Pedreschi R. A preliminary study of the strength of non-prismatic columns using fabric formwork. ResearchGate; 2015.
[7] He ZQ, Liu Z, Ma ZJ. Explicit Solutions of Transverse Tensions in Deep Beams: Load-Path Model and Superposition Principle. ACI Structural Journal. 2014;111(3):583-592.
[8] Al-Maliki HNG, Alshimmeri AJH, Ali AM, Madhloom HM, Gamil Y. Nonlinear Simulation Analysis of Tapered Reinforced Concrete Column (Solid and Hollow) Behavior Under Axial Load. International Journal of GEOMATE. 2021;21(86):131-146. https://doi.org/10.21660/2021.86.j2295
[9] Kadhim JA, Al-Zaidee SR. Numerical Simulation for Strength and Stability of RC Tapered Columns. Engineering, Technology & Applied Science Research. 2024;14(4):14819-14824. https://doi.org/10.48084/etasr.7228
[10] Head MC, Aristizabal-Ochoa JD. Analysis of Prismatic and Linearly Tapered Reinforced Concrete Columns. Journal of Structural Engineering. 1987;113(3):575-589. https://doi.org/10.1061/(ASCE)0733-9445(1987)113:3(575
[11] Aghayere AO. Design of Nonprismatic Concrete Columns by the Degree of Fixity Method. ACI Structural Journal. 1990;87(4):473-479. https://doi.org/10.14359/3099
[12] Manzelli AA, Harik IE. Prismatic and Nonprismatic Slender Columns and Bridge Piers. Journal of Structural Engineering. 1993;119(4):1133-1149. https://doi.org/10.1061/(ASCE)0733-9445(1993)119:4(1133
[13] Central Organization for Standardization and Quality Control (COSQC). IQS 5: Portland Cement. Baghdad: COSQC; 2019.
[14] Central Organization for Standardization and Quality Control (COSQC). IQS 45: Aggregate from Natural Sources for Concrete and Construction. Baghdad: COSQC; 2016.
[15] International Organization for Standardization (ISO). ISO 6935-2: Steel for the reinforcement of concrete - Part 2: Ribbed bars. Geneva: ISO; 2019.
[16] American Concrete Institute (ACI). ACI CODE-318-19: Building Code Requirements for Structural Concrete and Commentary. Farmington Hills (MI): ACI; 2019.
[17] Al-Rawe HS, Ahmed SY, Abdullah SM. Retrofitting of reinforced concrete columns under eccentric loads using enhanced ferrocement. Asian Journal of Civil Engineering. 2024;25:5727-5739. https://doi.org/10.1007/s42107-024-01141-6
[18] Benredjem A, Benredjem A, Chikh N, Mesbah HA, Benzaid R. Structural behaviour of square RC columns confined with CFRP wraps. MATEC Web Conf. 2018;149:02095. https://doi.org/10.1051/matecconf/201814902095
[19] Naji AJ, Naji AJ, Al-Jelawy HM, Saadoon SA, Ejel AT. Rehabilitation and strengthening techniques for reinforced concrete columns: review. J Phys Conf Ser. 2021;1895:012049. https://doi.org/10.1088/1742-6596/1895/1/012049
[20] Timoshenko SP, Gere JM. Theory of Elastic Stability. 2nd ed. New York: McGraw-Hill; 1961.
[21] Kupfer H, Hilsdorf HK, Rüsch H. Behavior of Concrete Under Biaxial Stresses. ACI Journal Proceedings. 1969;66(8):656-666. https://doi.org/10.14359/7388